ORIGINAL ARTICLES

3D phase diagram in vectorcardiography

Valeri Goussev*

Jewish Rehabilitation Hospital, Research Center, Laval, Quebec, Canada

Received: July 14, 2016 **Accepted:** August 31, 2016 **Online Published:** September 8, 2016
DOI: 10.5430/jbei.v3n1p1 **URL:** http://dx.doi.org/10.5430/jbei.v3n1p1

ABSTRACT

The article is intended to propose the new technique for analysis and visualization of vectorcardiograms based on the 3D phase diagrams. The regular Frank 3D lead system was considered as the signal source to construct 3D vector space. The three cardio signals from the lead system, representing the currents in the body, and the three integrated in time signals, representing the corresponding charge flows, were used to form 3D phase diagram. This diagram is considered as a new compact description of the dipole object properties in the 3D space, combining simultaneously information about the charge movements and the changes in values and orientation of the current. The regular properties, like the angular momentum of the charge flow and the dipole strength vectors and their covariance can be evaluated from the real vectorcardiogram. Based on the set of vectorcardiograms for 8 healthy controls and 7 myocardial infarction patients the 3D phase diagrams and their statistical parameters are evaluated and discussed. An example is given of the technique implementation for the comparison of the 3D phase diagrams in a control and a myocardial infarction patient.

Key Words: Phase diagram, Energy, Angular moment, Covariance, Rotation

1. INTRODUCTION

The electrocardiogram (ECG) as the resulting electrical activity of the myocardial cells and anisotropic fiber conductivity can be described in ways, which differ with their complexity and accuracy. The most advanced models, which are based on the electrodynamics of the myocardial activity in the electrically non-homogeneous torso compartments[1–3] and its finite element replacements,[4] give the detailed evoked electrical activity in the torso. However, they still suffer from the lack of the detailed description about the nonlinear mechanisms underlying the myocardial cell excitation and its propagation along the myocardium, which are the subjects of the more general approach based on the active tissues.[5–7] The simplified models, using the dipole representation of the potential driven currents in the homogeneous body tissues,[8,9] are also able to explain the detailed variations in ECG and are given preference in the cardiography due to their simplicity and clarity. More complicated models require a very intensive numerical processing support. When planning to visualize the propagation process on the computer screen, we need to consider the relatively simple model of the electrical activity in the myocardium. That's why we shall limit ourselves with the dipole model generated data, obtained from the orthogonal Frank lead system.[10,11] Instead of increasing the number of leads to get more information about the heart electrical activity we shall try to extract more information from the Frank lead system. This way we hope to have more simplified clinical implementation of the new technique, which will give more detailed information with the same number of leads. The fact, that the Frank lead system gives already a vector in 3D space, which can be directly plotted on the screen, was used to

*Correspondence: Valeri Goussev, Ph.D, D.Sc.; Email: valery.goussev@gmail.com; Address: Jewish Rehabilitation Hospital, Research Center, 3205, Place Alton Goldbloom, Chomedey, Laval, Quebec, H7V 1R2, Canada.

make 3D presentation of the vectorcardiograms (VCG) and to discuss their spatial properties.[1] As the VCG represents in some way the dynamical process of the excitation propagation along the myocardial cells, we extend the simple 3D VCG graph by its phase diagram, which also should have a 3D shape. The implementation of the 3D phase diagram technique to physiological data and its statistical evaluation was presented in the preliminary study of the gait.[12] This paper will provide a more detailed mathematical description of this technique and an illustration based on the real experimental data for the vectorcardiography. Beside the electrical activity of myocardial tissue the heart has also mechanical properties like the blood flow velocities in the different heart chambers, which can change with time along with VCG and can be measured independently. We hypothesized that, when considering more complex system combining the propagation of the electrical activity in the myocardium and the blood flow in the heart chambers, we need more then 3D space in the phase diagram representation of the dynamical properties for the whole complex system. So in reality for the detailed analysis of the complex heart dynamical system we need to use a phase diagram for more than 3D space.

2. METHODS

2.1 The VCG preprocessing

The raw Frank leads ECG recordings were taken from the Physiobank resource[13] for 8 healthy controls and 7 patients with diagnosis of the infarct myocardium (MI patients). Many recordings though had a low frequency baseline drift. So first we removed the drift from recordings applying the low pass Butterworth filter with the cutoff frequency 0.5 Hz, and subtracting then the filtered signal from the original recordings. We made the segmentation in every recording selecting the beginning of ECG signal at 300 ms before the R spike. Hence, the duration of ECG signals was assumed to be within the two beginning markers. All selected ECG signals were synchronized then[14] in such way that they were fitted to each other by scaling them in amplitude and scaling and shifting in time. The synchronized pattern of all ECG signals in the particular trial was considered as the ECG signal for further processing. The basic concept of the dipole evoked potential in the conducted media was used to explain the generation of the ECG potential:[8]

$$\phi(\mathbf{r}) = \frac{\mathbf{D}\cdot\mathbf{r}}{4\pi\sigma\cdot r^3} \tag{1}$$

where vector $\mathbf{r}$ (with components x, y, z) points to the observation point, $r = \|\mathbf{r}\|$, $\mathbf{D}$ (with components D_x, D_y, D_z) denotes the dipole strength vector, σ is the conductivity of the tissues, and $\phi(\mathbf{r})$ is the evoked potential at the observation point. As we know that every projection in the Frank lead system consist of two separate points, we can represent the ECG potential in the every projection as the difference of potentials (1):

$$V_k = \phi(\mathbf{r}_{k1}) - \phi(\mathbf{r}_{k2}) = \frac{\mathbf{D}}{4\pi\sigma}\cdot\left(\frac{\mathbf{r}_{k1}}{r_{k1}^3} - \frac{\mathbf{r}_{k2}}{r_{k2}^3}\right) \tag{2}$$

where $\mathbf{r}_{k1}$ and $\mathbf{r}_{k2}$ are two points on the axis, indicated with index k = 1,2,3 corresponding to one of axes in the Frank lead system, r_{k1} and r_{k2} are distances $r_{k1} = \|\mathbf{r}_{k1}\|$, $r_{k2} = \|\mathbf{r}_{k2}\|$, and V_k is the ECG potential measured between these two points.

Following the traditional considerations[8] we can rewrite equation (2) in the more concise form:

$$V_k = \mathbf{w}_k\,\mathbf{D} \tag{3}$$

where $\mathbf{w}_k = \frac{1}{4\pi\sigma}\left(\frac{\mathbf{r}_{k1}}{r_{k1}^3} - \frac{\mathbf{r}_{k2}}{r_{k2}^3}\right)$ is the scaling vector, which is depending only on the geometrical characteristic of the lead system and the conductivity. Now we make an association of the Frank lead system x, y, z with the indexed system k = 1,2,3 and we assume that the scaling vectors $\mathbf{w}_k$ are aligned with the 3 orthogonal axes of the Frank lead system. Hence, the reconstruction of the dipole vector $\mathbf{D}$ is the inverse problem of Eq.(3), unless the scaling vectors $\mathbf{w}_k$ are known. Having the exact solution for $\mathbf{D}$ as a trajectory in time, we can implement all developed further methods for analysis and diagnostics. However, the problem is that the scaling factors $\mathbf{w}_k$ are unknown and we can formulate only the approximate estimation of them based on the conventional setup of the Frank lead system. As we concern further more about reasonable diagnostic procedure, we need only the scaled copy of $\mathbf{D}$, so we expect that the possible small deviations of such approximation from the real position of vector $\mathbf{D}$ and the weights $\mathbf{w}_k$ will not affect seriously the diagnostic results. The main problem is to make the same scaling factors in all lead axes to ensure the similarity in orientation between scaled and real dipole vector $\mathbf{D}$. First we assume that the conductivity σ is the same in the space surrounding the dipole. Assuming the traditional orientation of axes x, y, z (x is in the frontal plane, directed to the left shoulder, y is in the frontal plane, directed to bottom, z is in the horizontal plane, directed backward), we make additional assumptions to equalize scaling in axes. We assume that the origin of the frame of reference is in the middle point of the dipole, then the observation points on every axis are in the

opposite direction and equally moved from the frame origin $\mathbf{r}_{i1} = -\mathbf{r}_{i2}$, the distances of the observation points from the frame origin are approximately equal for x and y axes: $r_{11} = r_{21} = d$, whereas this distance for z axis is smaller and we assume it to be $r_{31} = 0.75d$. The made assumptions correspond approximately the real lead system and let us discuss the real dipole strength vector properties with the same uncertainty when comparing healthy controls and MI patients.

Using these simplifications we get the scaling vectors $\mathbf{w}_k$ in the form: $\mathbf{w}_k = a\mathbf{e}_k$ for k = 1,2 and $\mathbf{w}_k = 2.25a\mathbf{e}_k$ for k = 3, where $\mathbf{e}_k$ are the unit vectors in x, y, z frame of reference, $a = \frac{1}{2\pi\sigma d^2}$ is the unified scaling factor. We consider ECG potentials V_i as the components of the ECG vector $\mathbf{V}$ given in the orthogonal frame of reference and we can rewrite Eq.(3) as:

$$\mathbf{V} = a \cdot M \cdot \mathbf{D} \tag{4}$$

where M is the diagonal matrix with the main diagonal: {1,1,2.25}. Denoting $\mathbf{U} = M^{-1} \cdot \mathbf{V}$, we have the new presentation of the ECG potential with uniformly scaled dipole strength vector: $\mathbf{U} = a \cdot \mathbf{D}$.

We can call the vector $\mathbf{U}$ as the corrected ECG recording vector (units: V), which is similar to the scaled dipole strength vector $\mathbf{D}$ (units: A*m) and, because of the constant conductivity, can be also considered as the scaled current evoked by the dipole strength vector. Within made suppositions both vectors $\mathbf{U}$ and $\mathbf{D}$ keep the same orientation in space and differ only in the magnitude and units. We also define the scaled charge flow $\mathbf{Q}$ as the time integral of the corrected ECG vector: $\mathbf{Q} = \int_0^t \mathbf{U}\mathrm{d}t$, which is the scaled from the real charge flow with the same scaling factor a. Both uniformly scaled vectors $\mathbf{U}$ and $\mathbf{Q}$ will be further referred as the scaled dipole strength vector and the scaled charge flow vector.

2.2 The *n* dimensional phase diagram

The phase space trajectory is a most general way to represent all dynamic properties of a given dynamic system.[15] However, the graphic presentations of space trajectories for high n dimension systems can be highly confusing. For $n = 1$ the simplest way to display the phase trajectory is to build the phase diagram, which is usually associated with Lissajou's figure.[16] In spite of that the phase diagrams are widely used to visualize the internal relationship between dynamical system compartments in biomedical studies,[17] this technique cannot be easily extended for the higher dimension spaces. Even though the visual presentation of the phase diagrams is supposed to be limited to 2 or 3 dimensional spaces, we shall describe their properties for n dimensional space, because the numerical values can be investigated independent of their visual representation or the visual representation can be taken selectively from the set of all available coordinates. Along with VCG dynamics trajectories we consider some integral characteristics like the kinetic and potential energy distribution between coordinates, and the charge flow trajectory parameters like the angular moment, and covariation between projections of the dipole strength vector. When deriving the properties of n dimensional phase diagram and trajectory parameters we will keep the traditional terminology using coordinates and velocities and referring them later in the VCG interpretation as the charge flows and the dipole strength vectors.

Firstly, we introduce the complex vector space $\Omega = E_n \times E_n$ with column vectors $\mathbf{w} = \{q_k + ip_k\}_{k=1}^n$, where $i = \sqrt{-1}$. Similar to the phase space trajectories, any phase diagram of a dynamic system can be represented as the vector $\mathbf{w}(t)$ composed with q_k and p_k being the generalized coordinates and their velocities. We consider only periodic phase trajectories related to the stable dynamic system, depending on time $t \in [0, T]$, where T is the recurrent time of the phase trajectory and the observation time. We suppose also that all components of vector $\mathbf{w}(t)$ are belonging to Hilbert space $\mathbf{w}(t) \in L_2(0, T)$. We now define the phase diagram as the vector field Λ, which contains the manifold K, composed of coordinates $\mathbf{q} = \{q_k\}_{k=1}^n$ and velocities $\mathbf{p} = \{p_k\}_{k=1}^n$ derived at every point q_k at the time t. Vector $\mathbf{p}$ is tangent to the trajectory drawn by vector $\mathbf{q}$ in time. Therefore, in the graphic displays for even low dimensions of n (for example 2 or 3) both the trajectory fragment and the velocity vector locally coincide. Now, let us consider the specific circular vector transformation in E_n. This can be achieved by multiplying the coordinate vector with the transformation matrix A:

$$A = \begin{pmatrix} 0 & 0 & * & * & -1 \\ 1 & 0 & * & * & 0 \\ 0 & 1 & * & * & 0 \\ * & * & * & * & * \\ 0 & * & * & 1 & 0 \end{pmatrix} \tag{5}$$

The matrix can be considered as a rotation for even $n|A| = 1$, and as a reflection for odd $n|A| = -1$. Next, we transform circularly m times the velocity vector $\mathbf{p}$ using matrix A, such that the new velocity vector $\mathbf{v}$ is $\mathbf{v} = A^m\mathbf{p}$. m is called the order of transformation, so that $A^m = \prod_{j=1}^m A$ (we assume also that A^0 is the identity matrix).

Property 1 of matrix A: For any vector $\mathbf{p} \in E_n, A^n\mathbf{p} = -\mathbf{p}$.

Proof: Consider m sequential transformations of vector $\mathbf{p}$ by matrix A: $\mathbf{v} = A^m\mathbf{p}$. It is sufficient to consider only $m \in [1, n]$. Matrix A shifts circularly projections of vector $\mathbf{p}$ to the next axis assigning the very first projection the negative sign. After m transformations we have:

$v_k = p_{k-m}$ when $k > m, v_k = -p_{k+n-m}$ when $k \leq m$. So for $m = n$ we get immediately $v_k = -p_k$.

Property 2 of matrix A: For any vector $\mathbf{p} \in E_n$ matrix $G = A^{n/2}$ (for even n) and matrix $G = (A^{(n-1)/2} + A^{(n+1)/2})$ (for odd n) transforms the vector $\mathbf{p}$ to the orthogonal vector $\mathbf{v}$.

Proof: For the even n we have for $m = n/2 : v_k = p_{k-n/2}$ when $k > n/2$ and $v_k = -p_{k+n/2}$ when $k \leq n/2$. Evaluating the scalar product $\mathbf{v}' \cdot \mathbf{p} = \sum_{k=n/2+1}^{n} p_{k-n/2} \cdot p_k - \sum_{k=1}^{n/2} p_{k+n/2} \cdot p_k$ we see that both sums contain the same products and hence $\mathbf{v}' \cdot \mathbf{p} = 0$ what proves the orthogonality for the even n. For the odd n we consider the sum of transformation by two matrixes with $m1 = (n + 1)/2$ and $m2 = (n - 1)/2$. After transformations with $m1, m2$ we have two output vectors: the first $v_k = p_{k-(n+1)\cdot 2}$ when $k > (n + 1)/2$ and $v_k = p_{k+(n+1)/2}$ when $k \leq (n + 1)/2$ and the second: $w_k = p_{k-(n-1)\cdot 2}$ when $k > (n - 1)/2$ and $w_k = -p_{k+(n-1)/2}$ when $k \leq (n - 1)/2$. Evaluating the scalar product $\mathbf{p}'(\mathbf{v}+w) = \sum_{k=(n+1)/2+1}^{n} p_k(p_{k-(n+1)/2} + p_{k-(n-1)/2}) - \sum_{k=1}^{(n-1)/2} p_k(p_{k-(n+1)/2} + p_{k-(n-1)/2})$ we see that sums contain again the same products, what results in $\mathbf{p}' \cdot (\mathbf{v} + w) = 0$ and the orthogonality for the odd n.

Implementing twice Property 1 to vector $\mathbf{p}$ we get $A^{2n}\mathbf{p} = \mathbf{p}$. For Property 2 we can make additional remarks that for even n matrix G is the rotation matrix and, hence, preserves the norm of the vector $\mathbf{p}$. For odd n matrix G is the antisymmetric matrix and to keep the norm of the vector $\mathbf{p}$ unchanged we need an additional scaling, so, in condition $\|G\mathbf{p}\| > 0$, the new orthogonal vector $\mathbf{v}$ can be expressed as $\mathbf{v} = \frac{G\mathbf{p}}{\|G\mathbf{p}\|} \|\mathbf{p}\|$. Using Property 2 to make the orthogonal velocity vector we get the new phase diagram vector $\mathbf{u} = \{q_k + iv_k\}_{k=1}^{n}$, where the velocity vector does not coincide with the tangent velocity of the trajectory and hence will be visually distinguishable from the trajectory itself. The additional rotation of the vector velocity was intuitively used in one dimensional phase diagram (Lissajou's figures), where the one dimensional space is embedded in the two dimensional space and the symbol $i = \sqrt{-1}$ is associated with the velocity rotation by 90 deg. We extended this idea to the n dimensions and for even n the matrix G is the exact replacement of the symbol $i = \sqrt{-1}$ in the formulation of the high order spaces. For the odd n, similar to Lissajou's way, we can extend the space dimension by one, making the new space, which has only rotation matrixes. However, for simplicity of explanation of the charge flow parameters in the available data set in the scope of this article we'd remain in the 3D space. Among those parameters we consider the angular momentum and the covariance, which are described below for the n dimensional space.

2.3 Circular covariance

Let $\mathbf{p}$ and $\mathbf{v}$ are the velocities of the trajectory given by coordinates $\mathbf{q} = \{q_k\}_{k=1}^{n}$. The covariance (the outer product) between vectors $\mathbf{p}$ and $\mathbf{v}$ is described by a covariance matrix $R = \{r_{jk}\}_{j=1,k=1}^{n}$, where $r_{jk} = \frac{1}{T}\int_0^T p_j \cdot v_k \mathrm{dt}$ and T is the observation time. Usually, when dealing with dynamic systems we don't consider the pure statistical sense of the covariance, but rather the alignment between projections in the movement. High values of the covariance are associated then with high aligned projections. In contrast, low values of covariance will refer to the high orthogonality or discordance between the projections.

We need a particular form of matrix R containing dependence on the transformation matrix A, so we start with the following definition:

$$R_m = \frac{1}{T}\int_0^T \mathbf{p} \cdot \left(A^m\mathbf{p}\right)' dt \tag{6}$$

where ()' is the transposition operator, and R_m is the circular covariance matrix for the original and m - times transformed vectors.

We define the m order circular covariance C_m from the matrix R_m as:

$$C_m = Tr(R_m) = \frac{1}{L}\int_0^L (A^m\mathbf{p})' \cdot d\mathbf{q} = \frac{1}{T}\int_0^T (A^m\mathbf{p})' \cdot \mathbf{p}\, dt = \frac{1}{T}\int_0^T \|\mathbf{p}\|^2 \cdot Cos(\alpha_m) dt \tag{7}$$

where $Tr(R_m)$ is the trace of matrix R_m, L is the length of the trajectory, $d\mathbf{q}$ is the element of the trajectory given by vector $\mathbf{q}(t)$, α_m is the angle between vectors $\mathbf{p}$ and $A^m\mathbf{p}$, $\alpha \in [0, \pi]$. We can say also that C_m is the mean circulation of the vector $A^m\mathbf{p}$ over the trajectory $\mathbf{q}(t)$. As the order m is the incrementing step when circularly incrementing indices inside interval [1, n], it represents the neighborhood distance between coordinates when calculating the covariance. We can represent the covariance C_m:

$$\delta_{vm} = \frac{1}{T}\int_0^T \frac{\mathbf{p}' \cdot A^m \mathbf{p}}{\|\mathbf{p}\|^2} dt = \frac{1}{T}\int_0^T Cos(\alpha_m) dt \tag{8}$$

In the case of no rotation by matrix A, then (m=0), $\mathbf{v} = \mathbf{p}$ and the value C_0 is the mean total kinetic energy along the trajectory $\mathbf{q}(t)$ related to the doubled unit mass. Almost the same way can be used to define the covariation and its parameters for the trajectory $\mathbf{q}(t)$.

2.4 Angular momentum

We consider the movement of every point in the trajectory as consisting of two parts. The first one relates to the angular momentum of the point relative the frame of reference. The second one, the radial trajectory movement is directed along the coordinate vector of the point. We start to derive the angular momentum from the outer product B of the coordinate vector $\mathbf{q}$ and velocity vector $\mathbf{p}$ taken from every time point of the movement trajectory: $B = \mathbf{q} \cdot \mathbf{p}'$. The trace of matrix B contains the scalar product of $\mathbf{q}$ and $\mathbf{p}$, which is the part of the radial trajectory movement, whereas all non diagonal elements relate to the angular momentum. We can say that the angular momentum is distributed over $n(n-1)$ elements of matrix B excluding the main diagonal, which belongs to the radial movement. Subtracting from $\mathbf{p}$ its part, which is aligned with $\mathbf{q}$, we get vector $\mathbf{c}$:

$$\mathbf{c} = \mathbf{p} - \mathbf{q} \cdot (\mathbf{q}' \cdot \mathbf{p}) \cdot \|\mathbf{q}\|^{-2} \tag{9}$$

which is orthogonal to $\mathbf{q}$. Matrix $M = \mathbf{q} \cdot \mathbf{c}'$ has its trace equal zero and contains now only the angular momentum distribution. The real magnitude g of the angular momentum M is given by the Frobenius norm of matrix M : $g = \|M\|_F$ and is equal to the product $g = \|\mathbf{q}\| \, \|\mathbf{c}\|$.

In the 3D space, we have the representation of angular momentum in the vector form $\mathbf{g} = \mathbf{q} \times \mathbf{p}$ like the particular cross product of vectors $\mathbf{q}$ and $\mathbf{p}$ along the trajectory and its matrix distribution M has exactly 3 values, which can be associated with projections of $\mathbf{g}$ on x, y, z axes.

2.5 Total energy distribution along the trajectory in the coordinate space

We will consider the Sobolev norms[18] for the vectors $\mathbf{w}$ and $\mathbf{u}$ as: $\|\mathbf{w}\|_{W^{1,2}_{0,T}} = \left(\int_0^T \mathbf{w}'\mathbf{w}^* \mathrm{dt}\right)^{1/2}$, where $\mathbf{w}^*$ is the conjugate vector of $\mathbf{w}$. We will also consider the scalar product of two vectors as

$$\Psi_m = \frac{1}{T}\int_0^T \mathbf{w}'\mathbf{u}^* \, dt = \frac{1}{T}\int_0^T \mathbf{q}'(A^m\mathbf{q}) \, dt + \frac{1}{T}\int_0^T \mathbf{p}'(A^m\mathbf{p}) \, dt = \Pi_m + \Phi_m \tag{10}$$

where $\prod_m$ is the mean circular coordinate covariance distribution. Φ_m is the mean circular velocity covariance distribution along the number of coordinates. In absence of any rotation by matrix $A(m = 0)$ we have:

$$\Psi_0 = \frac{1}{T}\|\mathbf{w}\|^2_{W^{1,2}_{(0,T)}} = \Pi_0 + \Phi_0 \tag{11}$$

where $\prod_0$ and ϕ_0 are now the total mean potential and kinetic energies along the trajectory given by $\mathbf{q}(t)$, with ϕ_0 being the Soblolev norm divided by time T.

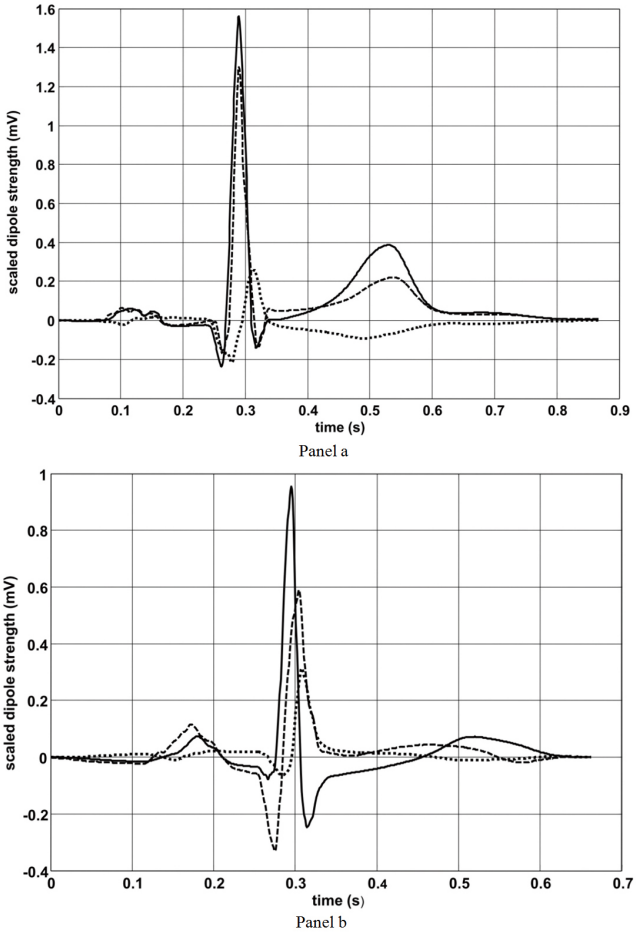

Figure 1. Corrected ECG in projections on x (solid), y (dashed), z (dotted) axes. Panel a – the healthy control, Panel b – the MI patient

3. IMPLEMENTATION AND RESULTS

The experimental data, related to 8 healthy controls and 7 MI patients, classified as infarct myocardium patients, were taken from the Physiobank resource.[13] The preprocessed VCG signals were integrated in time to get the charge flows, which were considered as the new space coordinates. All data processing was performed using Matlab and R (for statistical evaluation). As the real VCG data was available in digitized sequences of the length N related to the finite dimension space $l_2(N)$, all projection norms were replaced by the root mean square (RMS) calculated in the finite dimension space. For every healthy control and MI patients RMS, dipole strength, charge flows, angular momentum, and covariance were evaluated. For particular healthy control (file: cont117_s0292lre.xyz in the Physiobank resource) and the MI patient (file: pat11_s0039lre.xyz in the Physiobank resource) we show the full graphical representation of data. The preprocessed VCG recordings for the healthy control and the MI patient are presented on the Figure 1 (panel a and b correspondingly). The corresponding regular phase diagrams separately for every lead projections are given in the Figure 2 (panel a and b). Using developed 3D phase diagram approach the same set of regular phase diagrams can be represented as one 3D plot, which is presented in the Figure 3 (panel a and b).

Table 1. RMS, means for the scaled dipole strengths (mV)

	Φ_0	Φ_{0x}	Φ_{0y}	Φ_{0z}	m_{dx}	m_{dy}	m_{dz}
Group mean and std for controls							
Mean	0.26728*	0.22558*	0.1210	0.0584	0.07238*	0.0418*	-0.0086
std	0.061965	0.05071	0.06169	0.01757	0.03252…	0.02573	0.01809
Group mean and std for MI-patients							
Mean	0.16646*	0.11663*	0.0923	0.0660	0.01689*	-0.0048*	0.0042
std	0.04177	0.02137	0.05086	0.01153	0.02493	0.03562	0.01808

Table 2. RMS, means for the scaled charge flow (mV s)

	Π_0	Π_{0x}	Π_{0y}	Π_{0z}	m_{cx}	m_{cy}	m_{cz}
Group mean and std for controls							
Mean	0.05304*	0.0444*	0.0249	0.0096	0.0354*	0.0201*	-0.0033
std	0.0301	0.02551	0.01771	0.00948	0.0212	0.0144	0.0101
Group mean and std for MI-patients							
Mean	0.02222*	0.0142*	0.0118	0.0090	0.0069*	-0.0019*	0.0025
std	0.01404	0.0108	0.01171	0.00529	0.01238	0.0127	0.0078

All 3D plots can be considered as an embedding of a 6D space into a 3D space, containing 3 charge flow coordinates and 3 dipole strength variables. The difference compared to 3 conventional plots, is that each frame axis has now a double sense representing the coordinate and the dipole strength. To be able to see in the same time all details for two different vector entirety we had to scale down the dipole strength by the specific factor, which is kept constant between pictures to compare. Using the conventional technique, the phase diagram can relate only to one axis. However, as seen in Figure 2(a) and Figure 2(b), this procedure makes the 3D phase shape fragmented, and removes visible time interrelations between coordinates. In contrast the 3D phase diagram, keeps all coordinates and velocities in the scope of the same object. Tables 1, 2 provide the statistical analysis of RMS: $\Phi_0, \Phi_{0x}, \Phi_{0y}, \Phi_{0z}$ and means: m_{dx}, m_{dy}, m_{dz} for the scaled dipole strength as well as RMS: $\prod_0, \prod_{0x}, \prod_{0y}, \prod_{0z}$ and means: m_{cx}, m_{cy}, m_{cz} for the scaled charge flow.

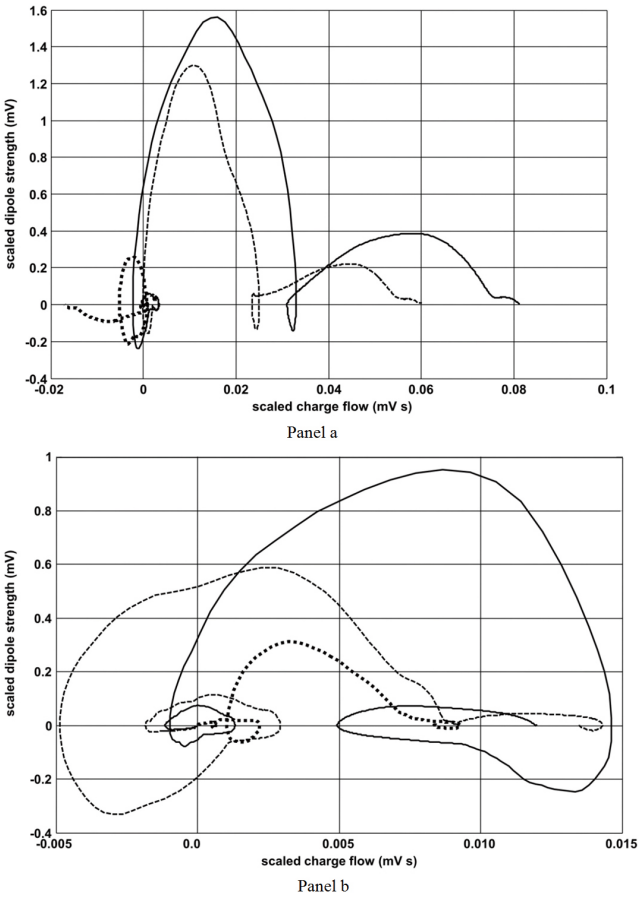

Figure 2. Regular phase diagrams separately drawn for x (solid), y (dashed), z (dotted) axes. The horizontal axis – scaled charge flow (mV s), the vertical axis – scaled dipole strength (mV). Panel a – the healthy control, Panel b – the MI patient

We normalize also charge flows and dipole strengths vectors before calculating the angular momentum, dividing them by the corresponding RMS. Table 3 contains the results of the statistical analysis of RMS: $\Gamma_x, \Gamma_y, \Gamma_z$ and means: m_{ax}, m_{ay}, m_{az} for the normalized angular momentum.

Table 3. RMS and means for the normalized angular momentum of the scaled charge flow trajectory (unitless)

	Γ_x	Γ_y	Γ_z	m_{ax}	m_{ay}	m_{az}
Group mean and std for controls						
Mean	0.23569	0.43892	0.38558	0.09907	-0.1702*	0.14834
std	0.07315	0.09419	0.0923	0.0491	0.02798	0.04733
Group mean and std for MI-patients						
Mean	0.35841	0.49756	0.47566	0.08860	-0.0963*	0.11348
std	0.15135	0.24007	0.12883	0.11555	0.048	0.09088

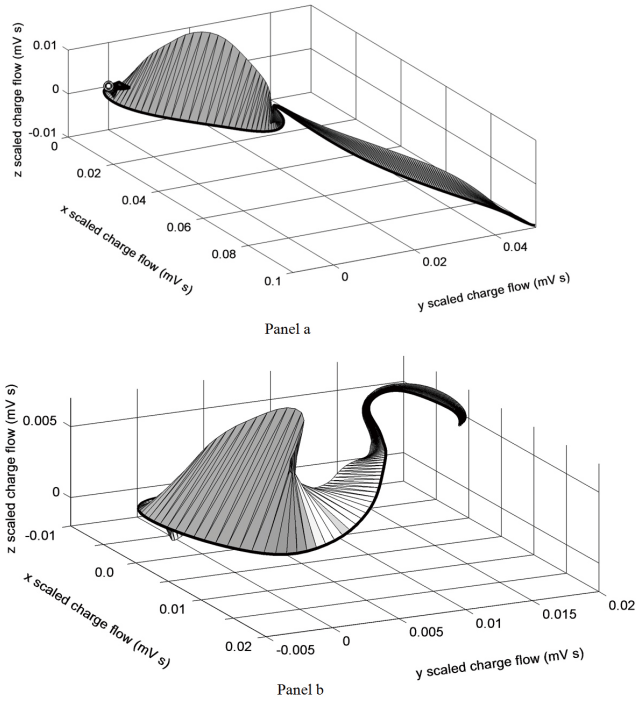

Figure 3. 3D phase diagram in x, y, z scaled charge flow frame of reference. The reducing scaling factor for the dipole strength vector is 0.01 (s). Panel a – the healthy control, Panel b – the MI patient

A stronger step to avoid any influences of the energies and amplitudes on interaction between projections of dipole strength and charge flow is to consider only the time dependence in projections. So we replaced all projections by their sign values in time.

$$R_p = \frac{1}{T}\int_0^T sign\,(\mathbf{p}\cdot(G\cdot\mathbf{p})')\,dt \tag{12}$$

$$R_q = \frac{1}{T}\int_0^T sign\,(\mathbf{q}\cdot(G\cdot\mathbf{q})')\,dt \tag{13}$$

The covariance distributions over coordinates x, y, z taken as the main diagonals from the covariance matrixes R_p and R_q between original and G matrix transformed vectors were statistically compared for healthy controls and the MI patients. The result is presented in the Table 4.

Table 4. Covariance between signed values of the regular and G transformed scaled dipole strength and scaled charge flow vectors (unitless)

	Scaled dipole strength			**Scaled charge flow**		
	x	**y**	**z**	**x**	**y**	**z**
Group mean and std for controls						
Mean	-0.34791	0.558048*	-0.50751*	-0.54853	0.65293*	-0.08761
std	0.49465	0.23467	0.19921	0.47869	0.29878	0.62353
Group mean and std for MI-patients						
Mean	-0.03121	0.10201*	-0.10314*	-0.41803	-0.02116*	0.28309
std	0.36066	0.32313	0.20181	0.56023	0.33674	0.691

The statistical analysis in all tables was performed using two tails regular T-test for those samples, where the samples successfully passed the Shapiro-Weil test for normality. For those samples, where the normality test failed, the Kolmogorov-Smirnov test was used. The parameters, which are denpted by the asterisks, are shown to be statistically different with the probability of error less than 0.05. The mean Sobolev norms Ψ_0 for the healthy controls 0.273291 ($\pm$0.065165) and for MI patients 0.168286 ($\pm$0.042491) are found to be statistically different.

4. Discussion

The mean values, RMS and energies are integral characteristics and are capable of describing all local changes, which can be seen only when watching the trajectories in time. However, the conventional way to analyze and make the conclusions in diagnostics is to consider the regular ECG visually. The proposed technique contributes to the conventional consideration an additional information channel containing the charge flow. This new feature allows visualizing the the combined information about the charge flow and the electrical current related to the dipole strength vector on the same picture. The information about ECG shape is still present in the combined picture and can be seen as a part of the common process of the electrical current propagation in the body. To see the particular shape details, the combined 3D object can also be rotated in the 3D view on the computer screen using the regular software. The analysis does not necessarily implicate the statistics. The essential part of any analysis of ECG and VCG is to find the associations between the particular shape of the raw recordings and the physical properties of the electrical current propagation in the myocardium. To facilitate this process it is highly desirable to visualize raw recordings in such way that almost all physical

properties were visible in the same graphical object. After having been successfully recognized such properties may be considered as the variables for the subsequent statistical analysis, which will make a selection of the reliable parameters suitable for diagnostics. In the present work we proposed for the analysis two basic physical properties for the analysis: rotation of the scaled charge trajectory and the alignment between projections of the scaled dipole strength current vector, which are associated correspondingly with the angular moment and the covariance considered both as parameters of VCG. The statistical comparison between healthy controls and MI patients, made on the small groups of the healthy controls and MI patients confirms the efficiency of the parameters to distinguish between the groups. The more essential data bases are needed to complete this study. Considering the particular statistical results we see that the energy related parameters (Sobolev norm, RMS for the charge flow, and dipole strengths) are higher in healthy controls. The more essential energy is concentrated in x axis (horizontal axis in the frontal plane). As we can see in the Tables 1 and 2 the healthy controls have energetically stronger dipole strength and charge flow vectors. Because of the energy dominance of healthy controls over the MI patients we expect to get also the essential difference in the angular momentum and the covariance between groups of controls and MI patients. This could attenuate others differences between groups if available. That's why we consider also the normalized charge flows and dipole strengths vectors before calculating the angular momentum. As we can see in the statistical comparison between control and MI patient groups given in the Table 3 the difference still exists in the mean values for the vertical coordinate. Taking into account the fact that RMS values for this axis are not shown to be statistically different, we can conclude that the vertical projection of the angular momentum in MI patients is changing its sign more frequently. For the diagnostic purposes we are more concerned about parameters of VCG, which are not depending on its energy and amplitude, as they can be easily modified by some external inputs, like the electrode contacts or gains of preamplifiers. So we consider also a specific transformation, which intends to make its result independent of the input amplitude and is defined like the signs of projection values in the scaled dipole strength and the scaled charge flow vectors. The covariance between signed values (see Eqs.12 and 13) reflects only changes in time. Nevertheless, the covariance, as seen in the Table 4, demonstrates an essential difference between groups of controls and MI patients. The fact that the significantly different covariances are less in MI patients is the evidence that the projections in the scaled charge flow and scaled dipole strength vectors are not aligned and have increased discordance between them.

5. CONCLUSION

The 3D phase diagram technique is an efficient way for the visualization and analysis of the myocardial electrical activity of the heart in 3D space. It allows embedding of the charge flow trajectories and dipole strengths currents in the same 3D space to build a unique object representing dynamical properties of the considered model of the myocardial electrical activity in its entirety. The normalized angular momentum and the dipole strength covariance parameters derived from the space trajectory are complementary to the 3D phase diagram and help to differentiate the electrical activity of the heart between the groups of subjects. The statistical and visual estimation of the 3D phase diagrams exhibits in the fully disclosed way the discordance in alignment between the projections in the scaled charge flow and scaled dipole strength vectors. The proposed phase diagram technique may be used as an effective tool for the visualization and analysis of trajectories in different space dimensions.

REFERENCES

[1] Yang H, Bukkapatnam STS, Kommanduri R. Spatiotemporal representation of cardiac vectorcardiogram (VCG) signals. Biomed Eng Online. 2012; 11: 16. PMid:22463593. http://dx.doi.org/10.1186/1475-925X-11-16

[2] Keener JP, Panfilov AV. A Biophysical Model for Defibrillation of Cardiac Tissue. Biophysical Journal. 1996; 71: 1335-1345. http://dx.doi.org/10.1016/S0006-3495(96)79333-5

[3] Clayton RH, Bernus O, Cherry EM, et al. Models of cardiac tissue electrophysiology: Progress, challenges and open questions. Prog Biophys Mol Biol. 2011; 104(1-3): 22-48. PMid:20553746. http://dx.doi.org/10.1016/j.pbiomolbio.2010.05.008

[4] Boulakia M, Cazeau S, Fernandez MA, et al. Mathematical Modeling of Electrocardiograms: A Numerical Study. Annals of Biomedical Engineering. Springer Verlag. 2010; 38 (3): 1071-1097. PMid:20033779. http://dx.doi.org/10.1007/s10439-009-9873-0

[5] Krinsky V, Pertsov A, Fast V, et al. A study of autowave mechanisms of cardiac arrhythmias. In: Nonlinear wave processes in excitable media. Ed. Holden AV, Markes M, Othmer HG. 1991: 5-14. http://dx.doi.org/10.1007/978-1-4899-3683-7_2

[6] Krinsky V, Pumir A. Models of defibrillation of cardiac tissue. Chaos. 1998; 8(1): 188-203. PMid:12779721. http://dx.doi.org/10.1063/1.166297

[7] Pumir A , Krinsky V. Unpinning of a rotating wave in cardiac muscle by an electric field. Journal of theoretical biology. 1999; 199(3): 311-319. PMid:10433895. http://dx.doi.org/10.1006/jtbi.1999.0957

[8] Oosterom van A. Vectorcardiography based analysis of atrial fibrillation, Electrocardiology. 2009: 39-55. (Proc 36th Int Congress on Electrocardiology, Wroclaw, Poland, Edts: M. Sobieszczańska, J. Jagielski and P.W. Macfarlane; JAKS Publishing Company 2010).

[9] Sameni R, Gari D, Clifford GD, et al. Multichannel ECG and Noise Modeling: Application to Maternal and Fetal ECG Signals. EURASIP Journal on Advances in Signal Processing. 2007, Article ID 43407: 1-14.

[10] Frank E. An Accurate, Clinically Practical System For Spatial Vectorcardiography. Circulation. 1956; 13: 737-749. PMid:13356432. http://dx.doi.org/10.1161/01.CIR.13.5.737

[11] Edenbrandt L, Pahlm O, Lyttkens K, et al. Vectorcardiogram more sensitive than 12-lead ECG in detection of inferior myocardial infarction. Clinical Physiology. 1990; 10: 551-559. PMid:2083483. http://dx.doi.org/10.1111/j.1475-097X.1990.tb00447.x

[12] Fung J, Patterson K, Perez C, et al. Vector space analysis of the body centre of mass movements to determine gait stability in normal and impaired locomotion. In: International Society for Posture and Gait Research (ISPGR) /Gait and Mental Function, 1st Joint World Congress. Trondheim, Norway. June 2012, Abstract # O.28.2. p.125-126.

[13] Goldberger AL, Amaral LAN, Glass L, et al. PhysioBank, PhysioToolkit, and PhysioNet: Components of a New Research Resource for Complex Physiologic Signals. Circulation. 2000; 101(23): e215-e220 [Circulation Electronic Pages; http://circ.ahajournals.org/cgi/content/full/101/23/e215] (June 13). PMid:10851218. http://dx.doi.org/10.1161/01.CIR.101.23.e215

[14] Åström M, Santos EC, Sörnmo L, et al. Vectorcardiographic Loop Alignment and the Measurement of Morphologic Beat-to-Beat Variability in Noisy Signals. IEEE Transactions on Biomedical Engineering. 2000; 47(4): 497-506. PMid:10763295. http://dx.doi.org/10.1109/10.828149

[15] Lanczos C. The Variational Principles of Mechanics,(Eds) Dover Publications; 4 edition. 1986. p.418.

[16] Pratt H, Bleich N, Har'el Z, et al. Three-channel Lissajous' trajectory of the human short latency visual evoked potentials. International Journal of Bio-Medical Computing. 1986; 18(3): 249-259. http://dx.doi.org/10.1016/0020-7101(86)90021-8

[17] Albuisson E, Alfieri R, Boire JY. Lissajous figures and visual electrograms by colored modulated stimulation, In: Engineering in Medicine and Biology Society, Images of the Twenty-First Century. Proceedings of the Annual International Conference of the IEEE Engineering. 1989; 4: 1219-1220.

[18] Sobolev SL. On a theorem of functional analysis. Transl. Amer. Math. Soc. 1963; 34 (2): 39-68; translation of Mat. Sb., 4 (1938), 471-497.